Supplementary Materials for

Nucleotide immune signal activates bacterial caspase by filament depolymerization

Xuzichao Li[1, 2, 3, #], Qiuqiu He[1, 2, #], Bin Liu[1, 2, #], Zhikun Liu[1, 2, #], Qian Zhang[1, 2], Xiaoshen Wang[1, 2], Tongyu Mao[1], Jie Han[1], Shuqin Zhang[1, 2], Fumeng Liao[1], Yingcan Liu[1], Zhengda Shan[1, 4], Zhenning Yin[1, 2], Yong Wei[3], Zhiyong Yuan[4], Hang Yin[1], Heng Zhang[1, 2, 4]*

1. State Key Laboratory of Experimental Hematology, Tianjin Medical University Cancer Institute and Hospital, Key Laboratory of Immune Microenvironment and Disease (Ministry of Education), The Province and Ministry Co-Sponsored Collaborative Innovation Center for Medical Epigenetics, National Clinical Research Center for Cancer, Tianjin Institute of Immunology, Tianjin's Clinical Research Center for Cancer, School of Basic Medical Sciences, Tianjin Medical University, Tianjin 300070, China
2. Tianjin Key Laboratory of Cellular Homeostasis and Disease, Key Laboratory of Cancer Prevention and Therapy, Department of Biochemistry and Molecular Biology, Tianjin Medical University, Tianjin 300070, China
3. Hangzhou Institute of Medicine, Chinese Academy of Sciences, Hangzhou, China
4. Department of Radiation Oncology, Tianjin Medical University Cancer Institute and Hospital, National Clinical Research Center for Cancer, Key Laboratory of Cancer Prevention and Therapy, Tianjin's Clinical Research Center for Cancer, Tianjin 300060, China.

# These authors contribute equally.

*Correspondence: zhangheng134@gmail.com (H.Z.)

Methods

Plasmid construction

The *caspase* gene encoding the full-length caspase protein (GenBank: WP_259418677) and the *tir* gene encoding the full-length TIR protein (GenBank: WP_001258751.1), derived from *Escherichia coli*, were cloned into appropriate expression vectors. The *caspase* gene was synthesized (Sangon) and inserted into the pET-derived vector containing an N-terminal His-MBP tag or His-Strep-Sumo tag. All plasmids were individually transformed into *E. coli* BL21 (DE3) cells for subsequent experiments. Point mutations were introduced using QuickChange mutagenesis (Takara) according to the manufacturer's protocol.

Protein expression and purification

The BL21(DE3) competent cells harboring the expression plasmids were plated on LB agar supplemented with the appropriate antibiotics. Single colonies were picked and inoculated into 4 mL LB medium for overnight growth at 37℃. The cultures were then expanded, and protein expression was induced with 0.2 mM isopropyl-β-D-thiogalactoside (IPTG) when the optical density at 600 nm reached ~0.6. Cells were subsequently cultured at 18℃ with orbital shaking at 180 rpm for 16 h. The resulting cell pellets were resuspended in lysis buffer (25 mM PBS pH 6.8, 150 mM NaCl, 5 mM imidazole, 5% glycerol, 2 mM β-mercaptoethanol) and lysed by sonication. The lysate was clarified by centrifugation to remove cell debris.

The supernatant was incubated with Ni-NTA resin, washed with buffer (25 mM PBS pH 6.8, 150 mM NaCl, 15 mM imidazole, 5% glycerol, 2 mM β-mercaptoethanol), depending on the tag of the target protein. Bound proteins were eluted with elution buffer containing 300 mM imidazole. TEV protease was utilized to remove the fusion tag. The target protein was loaded onto a HiTrap Q HP column (Cytiva) for ion-exchange chromatography. Peak fractions containing the target protein were concentrated and further purified by size-exclusion chromatography in gel-filtration buffer (25 mM MES pH 6.8, 150 mM NaCl, 2 mM DTT). Fractions were analyzed by SDS-PAGE to confirm protein identity and size. Correctly sized fractions were then concentrated, aliquoted, and stored at -80℃ until use. Tag-fusion proteins were purified using the same procedure, except that TEV protease was not added.

Phage plaque assay

Both *tir* and *caspase* genes were cloned into the pBAD-LIC (Addgene #37501) vector, and the recombinant plasmid was transformed into MG1655 cells for amplification. The overnight cultures were diluted 1:100 into semi-solid LB agar containing ampicillin and 0.2% L-arabinose (BBI), and overlaid onto solid LB agar for 1 h. T6 phage was serially diluted 10-fold in PBS, and 2 μL of each dilution was applied to the agar surface. After drying, the plates were inverted and incubated at 37℃ overnight. Plaque assays were performed in triplicate, and the resulting plaques were recorded and analyzed. The same strategy was applied to the mutants.

Spot assay

For the bacterial growth assay, both the type IV Thoeris system plasmid (8A) and the plasmid (pBAD33-Gm) containing mhp were constructed using a pBAD promoter, and the two recombinant plasmids were transformed into *E. coli* for amplification. Cells were cultured until the optical density at 600 nm reached ~0.3. After equal proportion dilution, these dilutions were spotted onto LB agar plates in the presence of 0.2% arabinose and the appropriate antibiotic. The plates were incubated overnight at 37°C and were imaged using a gel imager (Azure Biosystems).

The signaling molecule isolation

Reactions were carried out in a total volume of 200 μL containing 300 μM EcTIR protein, 6 mM NAD, and reaction buffer (25 mM MES pH 6.8, 150 mM NaCl, 2 mM DTT, 5 mM $MgCl_2$) and incubated at 37℃ for 1 h to generate signaling molecules via EcTIR-mediated NAD cleavage, followed by heating at 98℃ for 5 min to denature proteins. Insoluble proteins were then pelleted by centrifugation at 12,000 rpm for 30 min, and the clarified supernatant (200 μL) containing the resulting small molecules was transferred to HPLC for purification and isolation.

Semi-preparative HPLC was performed on a C18 column pre-equilibrated with the aqueous phase (5 mM ammonium acetate in water). The organic phase consisted of 5 mM ammonium acetate in 99% methanol. The gradient program was as follows: 0-30 min, 100% aqueous phase; 30-60 min, linear gradient from aqueous to organic phase; 60-80 min, 100% organic phase. The flow rate was maintained at 1 mL/min throughout. Elution was monitored by UV absorbance at 260 and 280 nm, and fractions corresponding to small molecule peaks were collected manually.

RT-qPCR

Cells expressing EcCaspase were cultured in LB medium at 37°C until the OD600 reached 0.5.

L-Arabinose was added to a final concentration of 0.2% to induce expression. T6 phage was added at an MOI of 0.01. The cells were infected for 30 min. Following infection, cells were harvested for total RNA extraction.

Total RNA was extracted using the RNApure Bacterial Kit (CoWin Biosciences), and cDNA was synthesized using StarScript III RT SuperMix (Genstar). RT-qPCR reactions were performed using 10 ng of cDNA and Real Star Fast SYBR qPCR Mix (Genstar). Gene expression was normalized using 5S rRNA as an internal control. All experiments were conducted with three biological replicates.

Biolayer interferometry assay (BLI)

The binding of N7-cADPR to wild-type EcCaspase and various mutant proteins was measured using the Octet RH16 system (Sartorius, USA). All experiments were conducted at 25 °C in black 96-well plates, with a total volume of 200 μL per well. His-MBP-tagged caspase proteins were immobilized onto Ni-NTA biosensor probes. The probes were prewetted in kinetic buffer (25 mM PBS pH 6.8, 150 mM NaCl, 0.02% Tween 20) and then loaded with wild-type or mutant caspase proteins (50 μg/mL). A set of sensors without protein was used as the background control. Both association and dissociation were monitored for all samples. Data acquisition and analysis were conducted using Octet software, with corrections for nonspecific binding, background signals, and signal drift performed using a double-reference subtraction method.

Native polyacrylamide gel electrophoresis (PAGE)

The sfGFP-N and sfGFP-C were each fused to EcCaspase at its N-terminus. The sfGFP-N-EcCaspase fusion construct was cloned into the pBAD-LIC vector (Addgene #37501), and the sfGFP-C-EcCaspase fusion construct was cloned into the pBAD33-Gm vector (Addgene #65098), both under the control of the endogenous promoter of the type IV Thoeris system. The recombinant plasmids were co-transformed into E. coli BL21(AI) competent cells.

Transformants were selected on LB agar plates with ampicillin (100 μg/mL) and gentamicin (50 μg/mL). Positive colonies were inoculated into LB liquid medium with the same antibiotics. Expression was induced with 0.2% L-arabinose, and the culture was grown to an OD600 of 0.5 at 37 °C, followed by T6 phage infection at an MOI of 4 for 3 hours.

Cells were harvested by centrifugation, resuspended in lysis buffer (25 mM MES pH 6.8, 150

mM NaCl, 2 mM DTT), and lysed by sonication. After centrifugation at 12,000 rpm for 10 min, the supernatant was mixed with non-denaturing loading buffer (without SDS or β-mercaptoethanol), and the reaction products were resolved by 4% non-denaturing PAGE in 0.5 × TBE buffer. The gel was imaged using a fluorescence imager (Azure).

Peptide cleavage reporter assays

Peptide cleavage reactions were carried out in a 100 μL volume containing tag-free EcCaspase or its mutants at 2 μM, a fluorescent peptide substrate at 5 μM, and N7-cADPR (Biolog Life Science Institute) at 2 μM in reaction buffer (25 mM MES pH 6.0, 150 mM NaCl). Each component was added sequentially and mixed gently. The reactions were transferred to a BeyoGold™ 96-Well Black Opaque Plate and monitored on a fluorescence microplate reader with excitation at 341 nm and emission at 441 nm. Fluorescence signals were recorded at 1-minute intervals for a total of 30 minutes to track substrate cleavage. Data shown represent fluorescence in the presence of N7-cADPR after subtraction of the corresponding background signal measured in the absence of N7-cADPR, unless otherwise indicated. The peptide cleavage reporter experiments were repeated at least three times.

LC-MS

A Strep-tag was fused to the N-terminus of EcTIR in the TIR-caspase system. *E. coli* K-12 MG1655 cells containing the TIR-caspase system were grown overnight at 37℃. The cultures were diluted 1:100 in LB with ampicillin and grown to an OD600 of 0.3. Induction was performed with 0.02% L-arabinose for 2 hours. T6 phage was added to the cultures at an MOI =1 for 1 h. Cells were collected and resuspended in Lysis buffer (25 mM MES pH 6.8, 150 mM NaCl, 2 mM DTT) and treated with 1 mg/mL lysozyme on ice for 30 min, followed by sonication. 1mL of lysate was incubated with Strep-Tactin beads for 2 h at 4℃. The beads were washed three times and then the bound proteins were eluted. The eluted samples were separated by a C18 column (75 μm inner-diameter×25 cm, 3 μm C18) and then electrosprayed directly on an Orbitrap Eclipse Tribrid mass spectrometer (Thermo Scientific). Spray voltage was set to 2.5 kV, funnel RF lens level at 40%, and ion transfer tube temperature at 320℃. Data were acquired using Xcalibur (v.4.5).

Escape mutant screening of T6 phage

T6 phage was mixed with WT host bacteria at different MOIs in melted soft-agar medium

(containing appropriate antibiotics and inducer) and poured onto pre-prepared solid agar plates, followed by overnight incubation at 37 °C. Single, clear plaques were picked and added to fresh host bacteria culture for amplification. The amplified mutant phages were serially diluted in PBS and spotted onto double-layer agar plates seeded with WT and empty vector control bacteria to confirm the escape phenotype. Wild-type T6 phage served as a control. Escape mutants formed clear plaques with similar titers on both WT and control lawns. Genomic DNA of successful escape phages was extracted and subjected to whole-genome sequencing.

Raw DNA-seq reads were processed using a standardized workflow based on established bioinformatics tools. Paired-end FASTQ files were merged and aligned to the indexed reference genome with BWA, and alignment outputs were converted, sorted, and indexed in BAM format using SAMtools[1]. Variants were identified with BCFtools through a unified calling model, and standard quality thresholds were applied to obtain a reliable variant set. Filtered VCF files were subsequently annotated with snpEff to characterize the functional impact of each mutation[2].

Negative stain electron microscopy

Samples (3.5 μL) were applied to carbon-coated copper grids that had been glow-discharged at 15 mA for 60 s and incubated for 1 min. For MBP-fused EcCaspase, samples were prepared at a concentration of 5 mg/mL, whereas tag-free EcCaspase samples were prepared at 1 mg/mL, unless otherwise indicated. Excess solution was removed by side wicking with filter paper. The grids were then stained with three successive drops of either 2% (w/v) uranyl acetate or phosphotungstic acid. The first two drops blotted away and the third left on the grid for 1 min before removal. Grids were air-dried at room temperature, stored in grid boxes, and imaged on a Thermo Scientific Talos L120C transmission electron microscope operated at 120 kV.

Cryo-EM sample preparation and imaging

For all EcCaspase complexes, 3.5 μL purified sample (1.0 mg/mL) was applied to glow-discharged Au R1.2/1.3 holey carbon grids (300 mesh, Quantifoil). Following a 10 s incubation, grids were blotted for 2 s at a blot force of 2, and then plunge-frozen into liquid ethane pre-cooled by liquid nitrogen, using Vitrobot Mark IV (FEI Thermo Fisher) at 4℃ and 100% humidity.

Datasets of all EcCaspase complexes were collected on a FEI Titan Krios microscope equipped with a Falcon4 detector at an acceleration voltage of 300 kV. Cryo-EM images were acquired at a

nominal magnification of 165,000×, corresponding to calibrated physical pixel sizes of 0.725, 0.731 and 0.692 Å/pixel, respectively. Images were recorded using EPU[3] with a defocus range of -1.2 to -1.6 μm. Each micrograph was dose-fractioned into 32 frames, with a total electron dose of 50 $e^-/Å^2$ per micrograph.

Cryo-EM data processing

For the dataset of MBP-fused EcCaspase complex, 7,225 micrographs were collected and processed in CryoSPARC[4]. Beam-induced motion was corrected with MotionCor2[5], and the contrast transfer function (CTF) was estimated. Micrographs with an estimated CTF resolution higher than 5 Å were excluded, resulting in 6,657 micrographs retained for further analysis. Particle picking was initially performed on 200 micrographs using blob picking, with a particle diameter range of 128-256 Å. One round of 2D classification was then conducted to remove junk particles. The retained high-quality particles were used to train a Topaz model[6]. Using this model for template-based particle extraction with a box size of 450 pixels, a total of 710,768 particles were extracted. Following rounds of 2D classification were applied to clean the particle stack. Ab-initio reconstruction generated initial volumes, one of which featured obvious protein secondary structures. Non-uniform refinement was conducted to further improve the quality of this promising map, achieving a final reconstruction at 2.84 Å resolution.

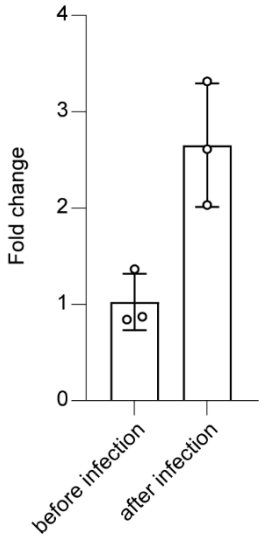
For the tag-free EcCaspase, 5,593 micrographs were processed using the same workflow. Particles were initially picked using the Blob picker and cleaned by several rounds of 2D classification, yielding 372,247 particles for subsequent analysis. These particles were subjected to ab-initio reconstruction and heterogeneous refinement. Non-uniform refinement yielded a reconstruction at 2.60 Å.

For the N7-cADPR-bound EcCaspase dataset, 6,417 micrographs were collected and processed using the same strategy described above. A total of 904,181 particles were extracted and subjected to 2D classification. The 2D class averages revealed that the particles existed not only as dimers but also assembled into tetrameric and hexameric forms. Initial volumes were obtained by ab initio reconstruction and further processed by rounds of 3D classification and heterogeneous refinement. Ultimately, 148,812 particles were subjected to non-uniform refinement, yielding a dimer reconstruction at 2.79 Å resolution. In addition, 54,124 particles produced a tetramer reconstruction

at 2.86 Å resolution, and 42,976 particles yielded a hexamer reconstruction at 2.89 Å resolution.

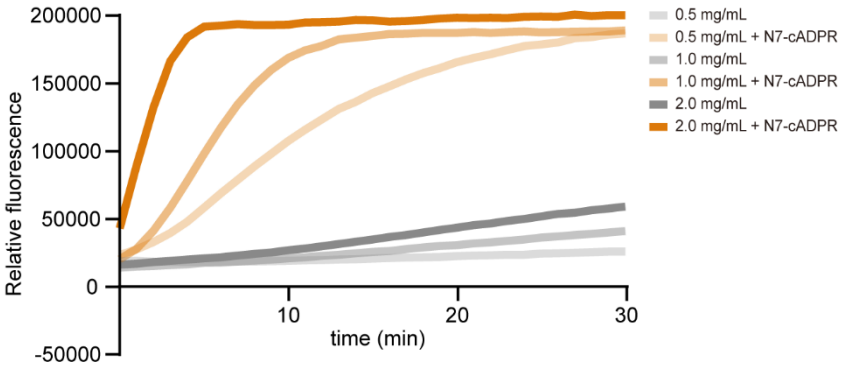
Model building and refinement

The initial atomic model of EcCaspase predicted by AlphaFold3[7] was manually divided into the NTD and CTD, which were individually fitted into the cryo-EM density map using ChimeraX[8] and subsequently connected into a single polypeptide chain. Copies of this model were positioned and manually refined to trace the density in Coot[9]. For modeling and refinement of the N7-cADPR molecule, a CIF restraint file was generated using eLBOW[10] in Phenix. After placement, manual adjustments were performed for both proteins and ligands to ensure correct geometries. Further refinements were performed by *phenix.real_space_refine*[11]. The quality of all final models was validated by MolProbity in Phenix[12]. Data collection and model refinement statistics are summarized in Supplementary Table S1.



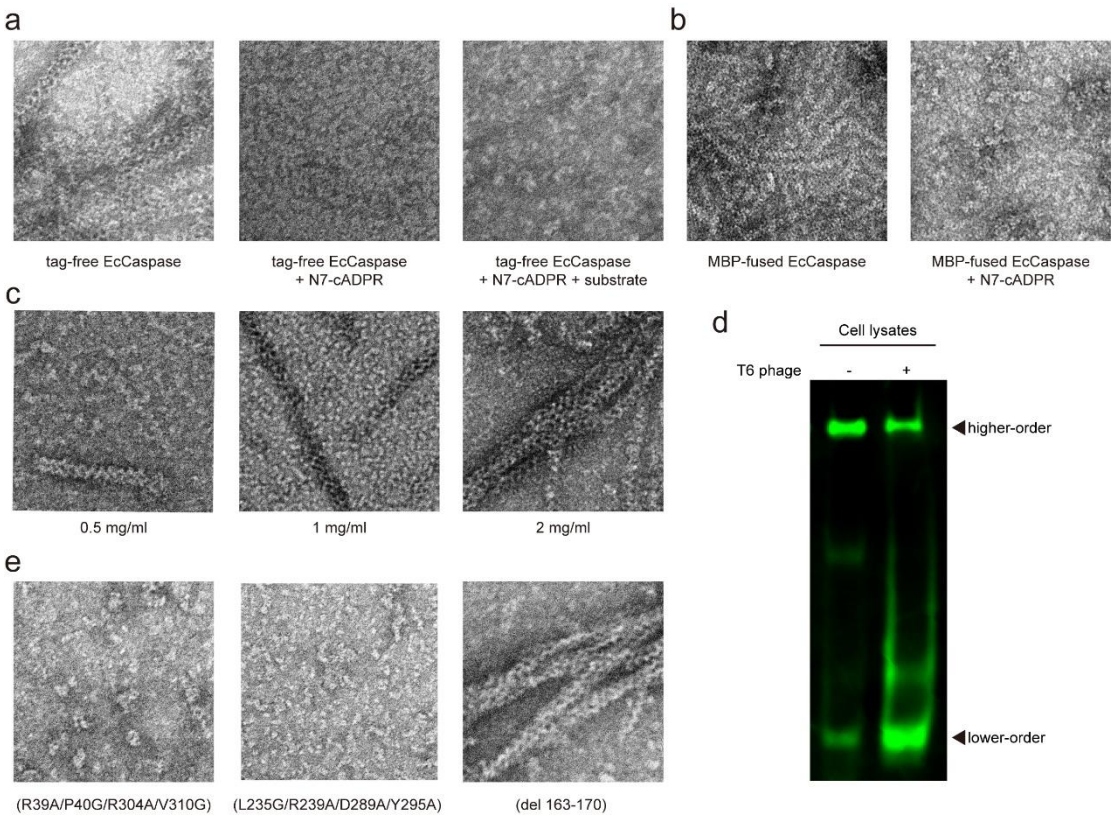
Supplementary Fig. S1 RT-qPCR quantification of mRNA in cell expressing type IV Thoeris system under T6 phage infection.

The mRNA levels of the type IV Thoeris system were quantified by RT-qPCR following T6 phage infection. Data are presented as mean ± SD (n = 3).



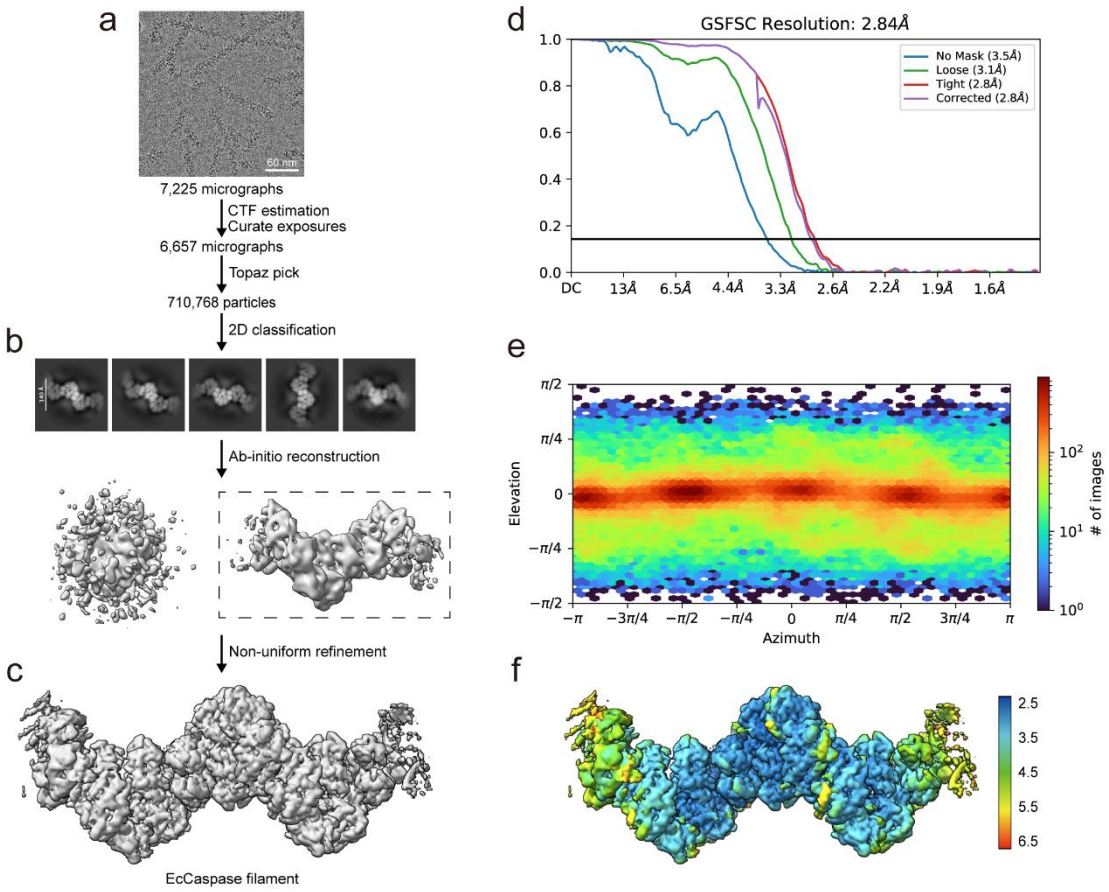
Supplementary Fig. S2 Peptide-cleavage reporter assays measuring EcCaspase activity at increasing concentrations.

Substrate cleavage activity of EcCaspase was measured over a range of protein concentrations. Data shown represent the raw fluorescence signal measured in the absence or presence of N7-cADPR.



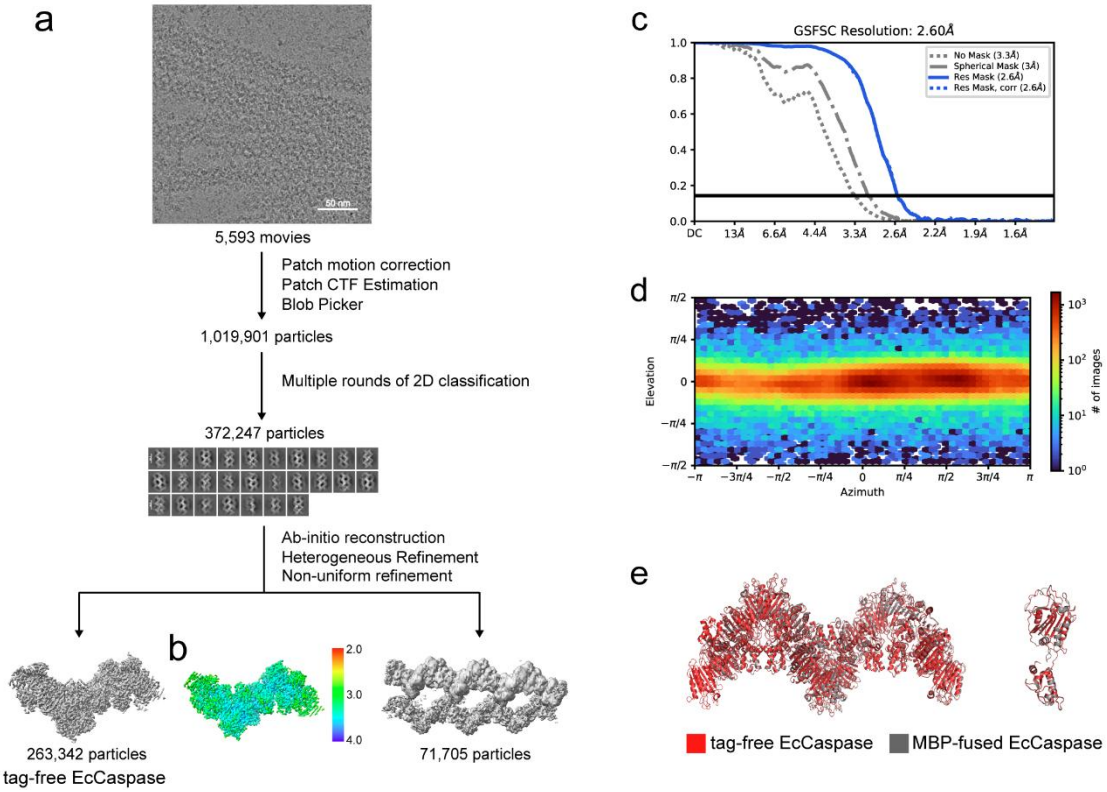
Supplementary Fig. S3 N7-cADPR activates the type IV Thoeris caspase through filament disassociation.

(a) Negative-stain EM micrographs of tag-free EcCaspase incubated with N7-cADPR or with both N7-cADPR and substrate. (b) Negative-stain EM micrographs of MBP-fused EcCaspase in the absence or presence of N7-cADPR. (c) Negative-stain EM micrographs of tag-free EcCaspase at protein concentrations of 0.5, 1, and 2 mg/mL. (d) Native PAGE analysis of cell lysates in the presence or absence of T6 phage infection. Representative gel from three replicates. (e) Negative-stain EM micrographs of the indicated tag-free EcCaspase mutants.



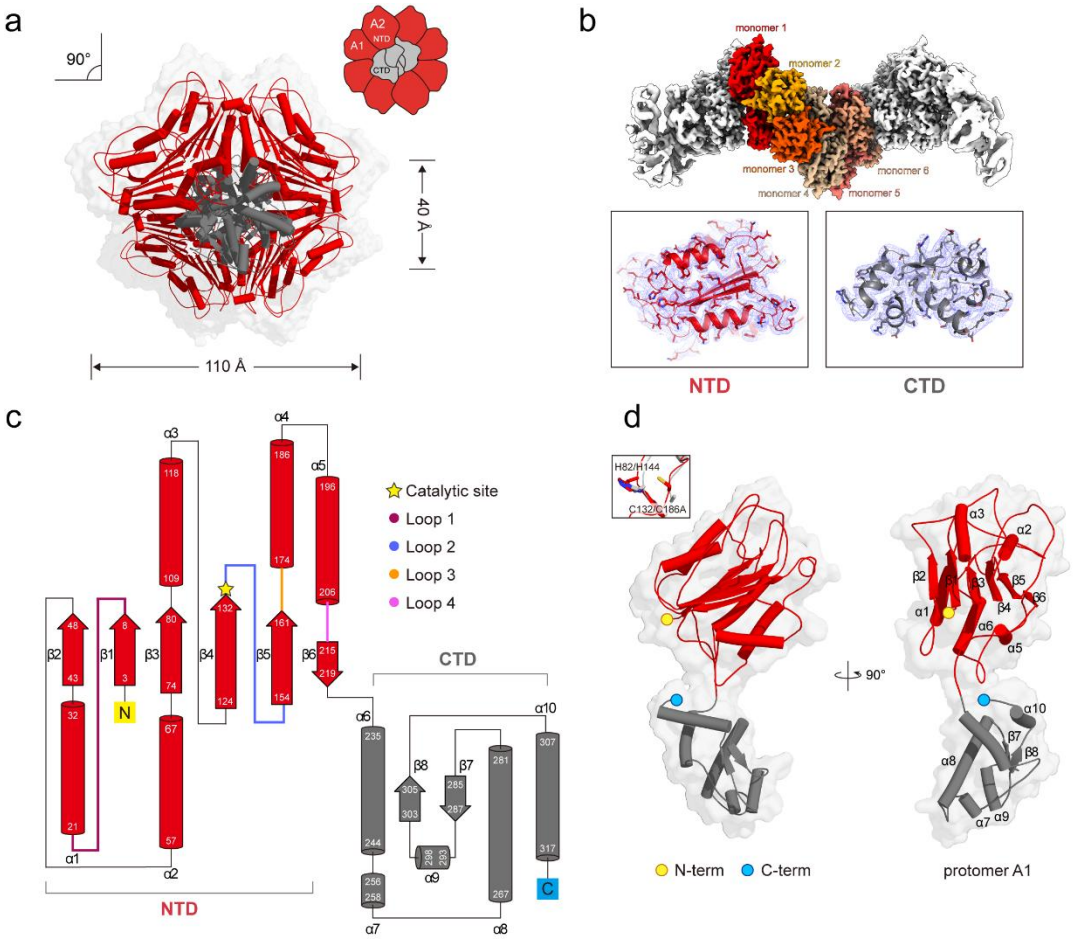
Supplementary Fig. S4 Cryo-EM data processing of MBP-fused EcCaspase filament.

(a) The workflow of data processing. (b) Representative 2D class averages of EcCaspase filament. (c) Final 3D reconstruction of EcCaspase filament. (d) Fourier shell correlation (FSC) curve. (e) Viewing direction distribution of the particles in the EcCaspase filament. (f) The resolution was estimated using the FSC = 0.143 cutoff.



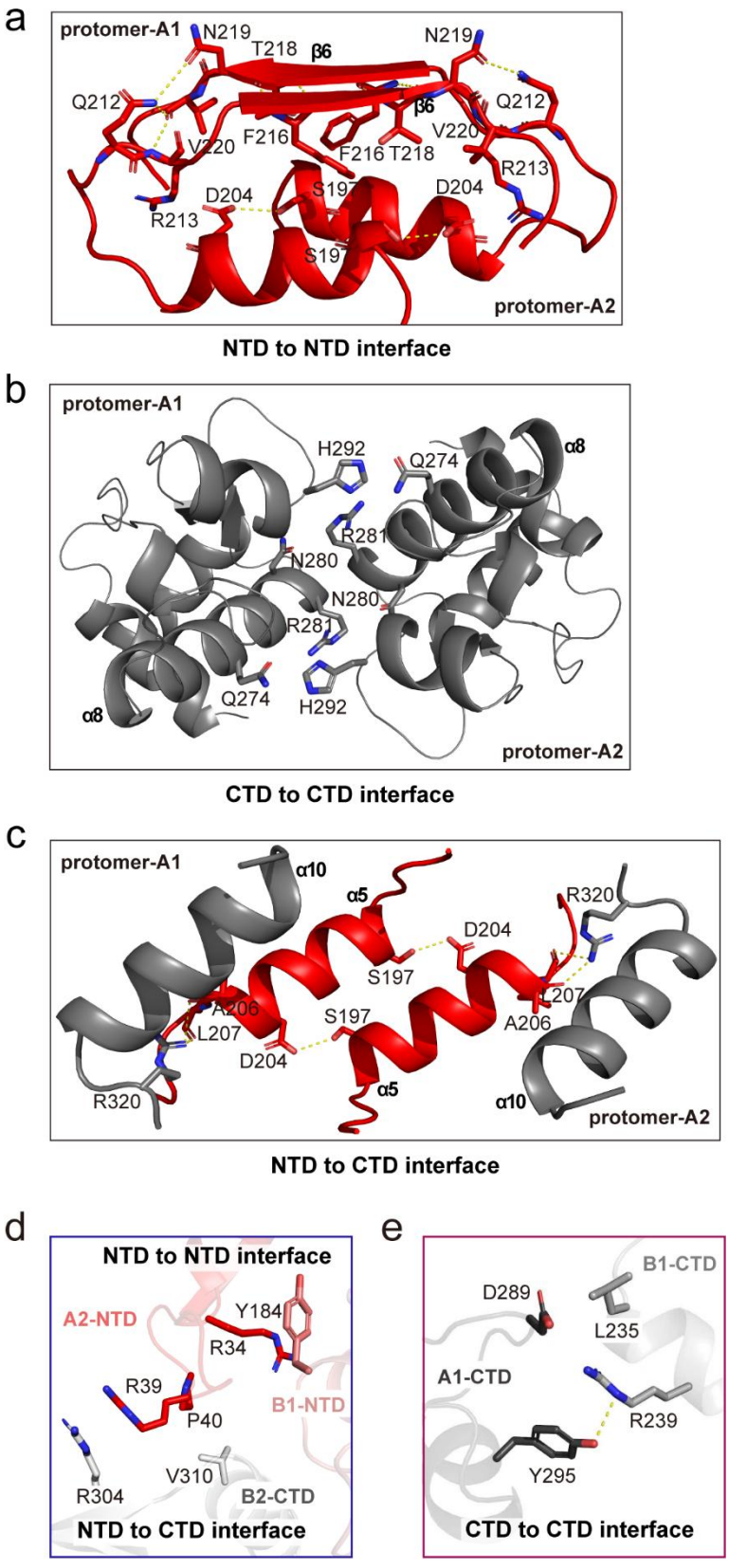
Supplementary Fig. S5 Cryo-EM data processing of tag-free EcCaspase filament.

(a) The workflow of tag-free EcCaspase filament data processing. (b) Final 3D reconstruction colored by local resolution. (c) Fourier shell correlation (FSC) curve. (d) Viewing direction distribution of the particles in the final reconstruction. (e) Structural comparison of tag-free and MBP-fused EcCaspase filaments.



Supplementary Fig. S6 Structural analysis of EcCaspase.

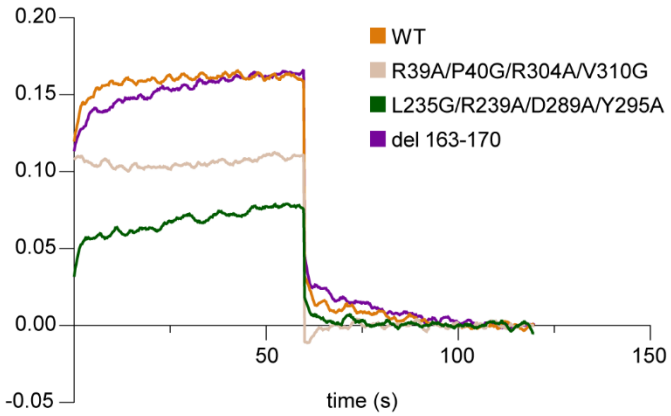
(a) Side view of the EcCaspase filament structure. Inserted panel presents a schematic model illustrating filament organization. The color scheme is consistent with Fig. 1a. (b) Upper panel shows the density map of EcCaspase filament. Six consecutive monomers are depicted with different colors. Lower panels represent the structures and corresponding cryo-EM density maps (shown as mesh) for the N-terminal and C-terminal domains of the EcCaspase protomer. (c-d) Topological diagram and atomic model of the EcCaspase protomer. Zoomed-in view of the active site alignment between EcCaspase and its human homolog (PDB ID: 1K88) is shown in the inset. Structural homology analysis using the DALI server showed that the NTD adopts an α/β fold characteristic of canonical caspases, closely resembling human caspase-4, -7, -8, -9, and -11, featuring a six-stranded β-sheet core (β1-β6) flanked by α-helices on both sides[13]. In contrast, no structural homologs were identified for the CTD, indicating that the CTD adopts a unique fold distinct from canonical caspases and may represent a Thoeris-specific structural innovation.



Supplementary Fig. S7 Structural basis of EcCaspase dimerization and filament assembly.

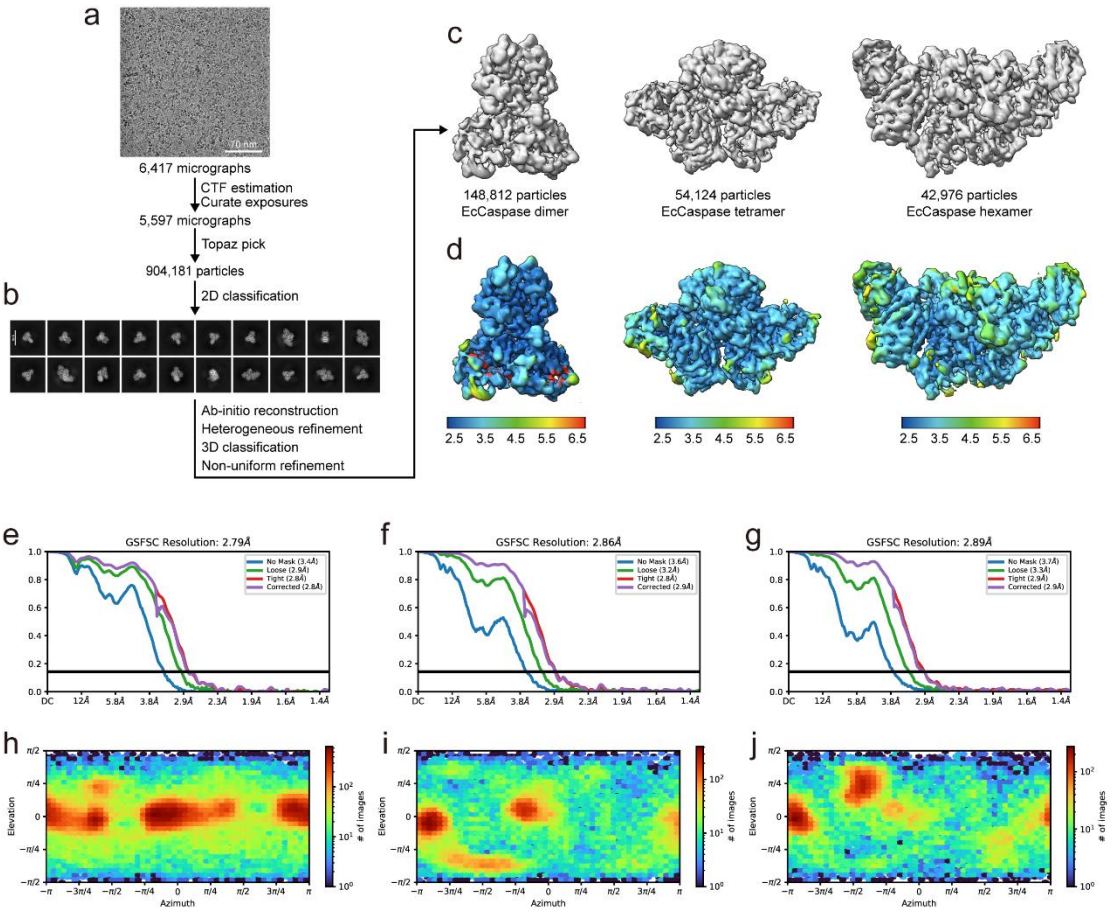
(a, b) Major intra-dimer interface is mediated by the two NTDs, which adopt an anti-parallel

arrangement, while the two CTDs protrude from the NTDs to pack face-to-face against each other, forming a V-shaped pocket with the potential to engage N7-cADPR. (c) Minor intra-dimer interface between NTDs and CTDs further reinforces the assembly of the dimeric asymmetric unit. (d) The NTD of protomer A2 mainly contacts the NTD of protomer B1, adopting a side-by-side conformation. In particular, the α1-β2 loop of A2 inserts into a pocket formed by B1 and B2, where Arg34 from protomer A2 stacks with Tyr184 of protomer B1 through a cation-π interaction. In addition, Arg39 and Pro40 from NTD of A2 pack against Arg304 and Val310 of protomer B2, establishing tight packing and hydrophobic interactions that further reinforce the filament architecture. (e) The two CTDs from one EcCaspase dimer unit associate with the other two CTDs from the adjacent dimer with two-fold symmetry, forming the CTD-CTD interface. In detail, Leu235 and Arg239 from α6 pack against Asp289 and Tyr295, respectively. For all panels, key residues mediating interactions are represented as sticks.

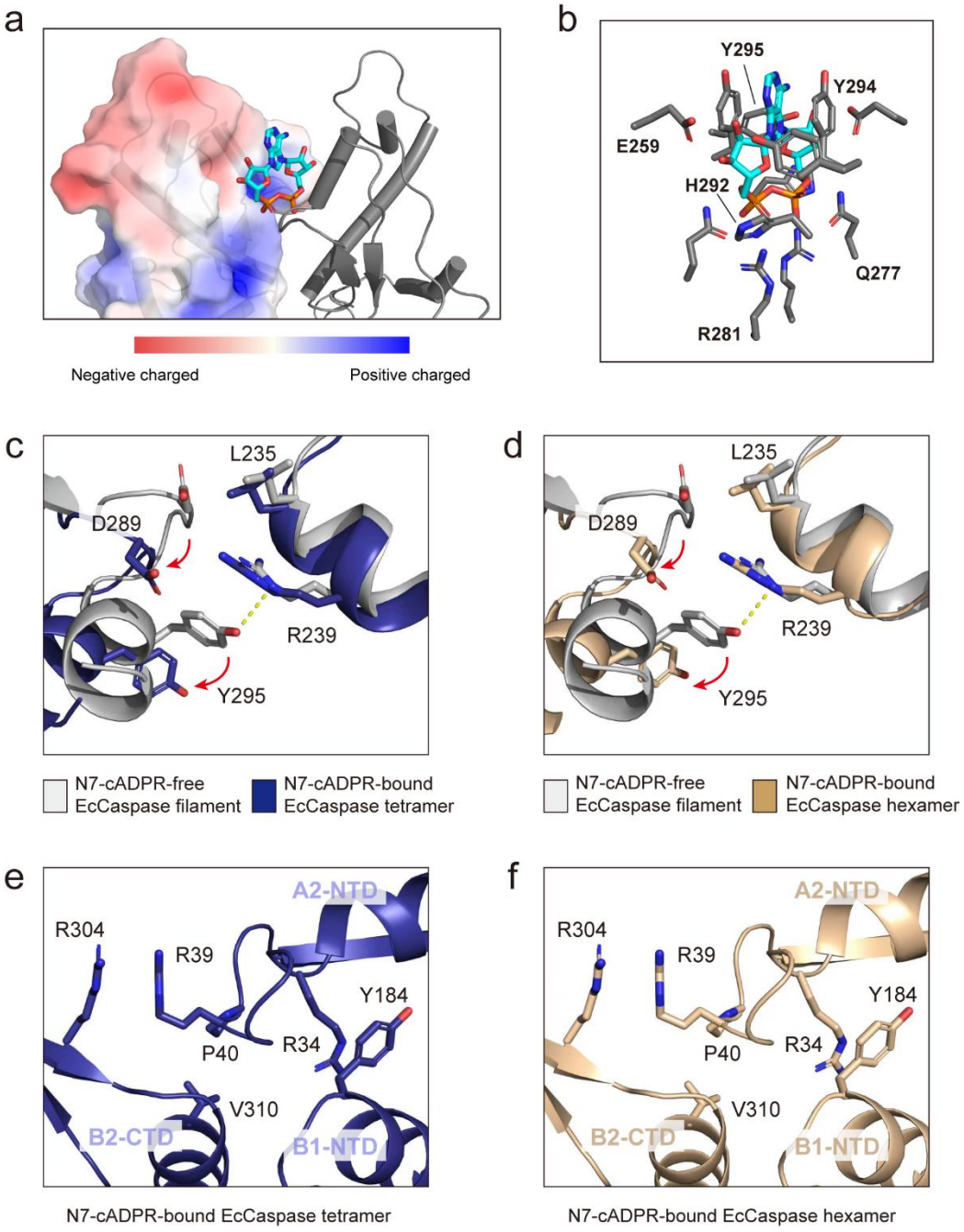


Supplementary Fig. S8 Biolayer interferometry analysis of N7-cADPR binding to EcCaspase and its variants.

Association and dissociation curves from representative BLI experiments showing interactions between N7-cADPR and EcCaspase or its variants.



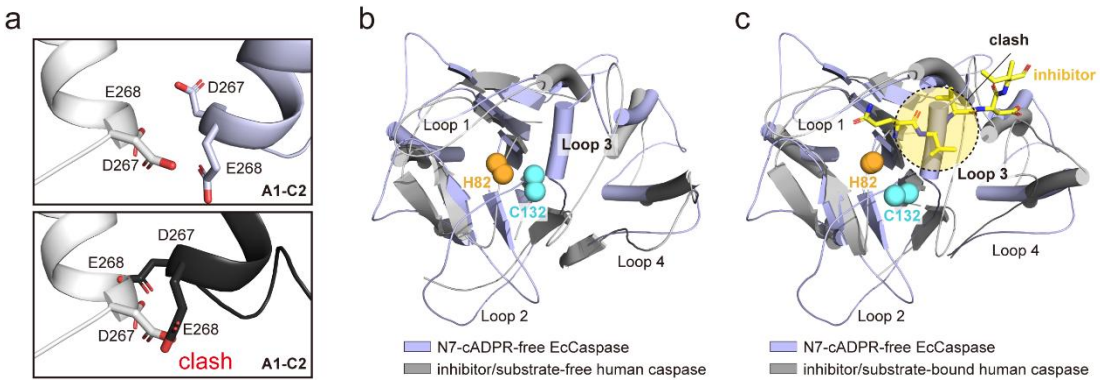
Supplementary Fig. S9 Cryo-EM reconstruction of N7-cADPR-bound EcCaspase complexes. (a) Cryo-EM image processing workflow. (b) Representative 2D class averages. (c) Final reconstructions of N7-cADPR-bound EcCaspase complexes. (d) Cryo-EM density maps colored according to the local resolutions. (e-g) Fourier shell correlation (FSC) curves, with overall resolutions of 2.79 Å, 2.86 Å, and 2.89 Å, were determined using the FSC = 0.143 criterion. (h-j) Angular distribution of selected particles for 3D reconstructions.



Supplementary Fig. S10 Ligand binding induces conformational changes.

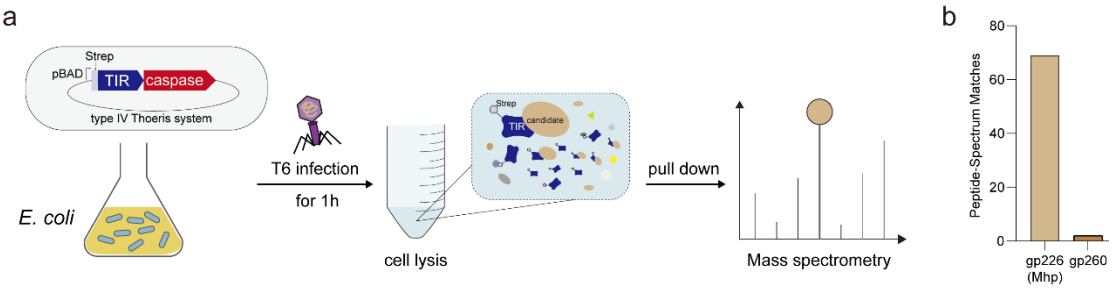
(a) Electrostatic surface representation of the ligand-binding pocket. N7-cADPR contains an adenine base, two ribose moieties, and two phosphate groups arranged in a cyclic configuration. The adenine and ribose parts are bracketed by the pocket walls, whereas the phosphates occupy the base of the binding pocket. (b) Interactions between N7-cADPR and the ligand-binding pocket. Specifically, the adenine ring is clamped by Tyr294 from both protomers through π-π stacking, while His292 and Tyr295 flip inward to stack over the ribose moieties, thereby enclosing the ligand. The

two Arg281 residues form a positively charged patch that establishes salt bridges with the phosphate groups of N7-cADPR. In addition, Glu259 and Gln277 residues from each CTD donate hydrogen bonds to the phosphates, further stabilizing N7-cADPR anchoring. (c, d) Ligand-induced conformational rearrangements disrupt CTD-CTD interactions. (e, f) NTD-NTD interfaces of N7-cADPR-bound EcCaspase tetramer and hexamer interactions. For all panels, interacting residues are shown as sticks.



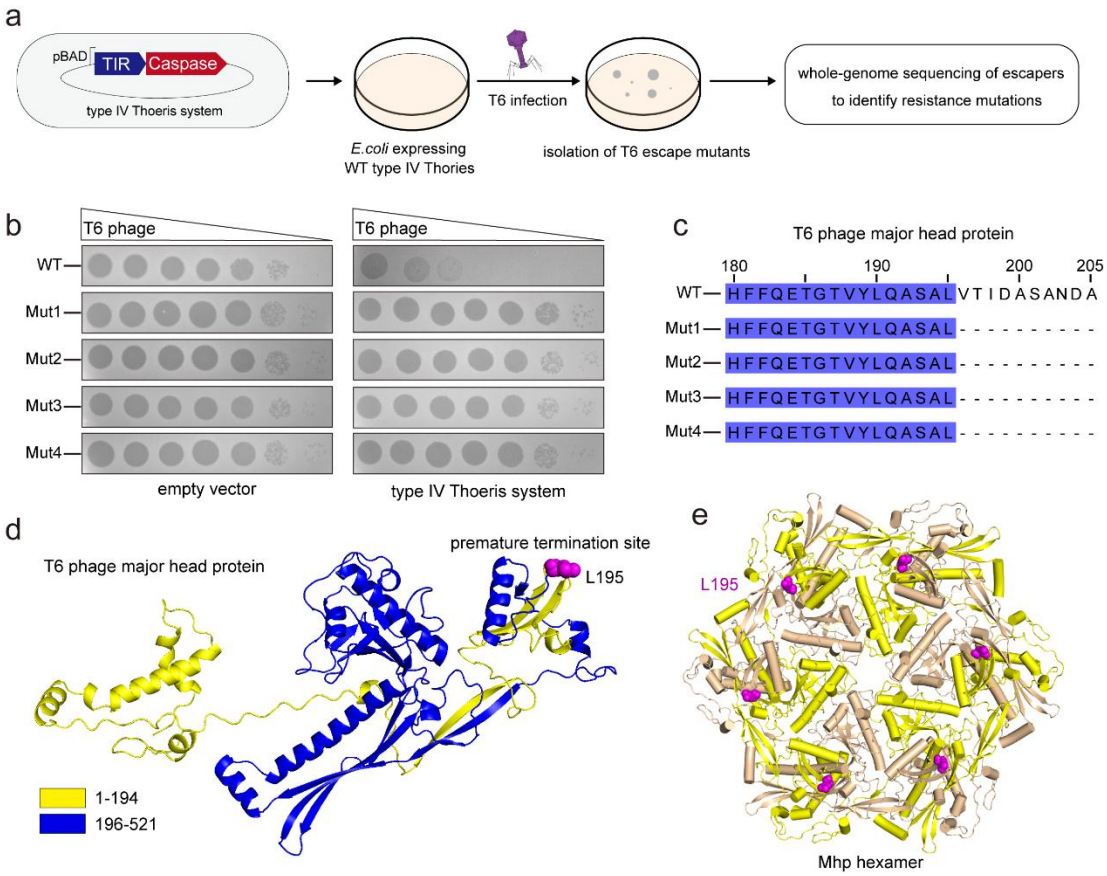
Supplementary Fig. S11 Structural basis for EcCaspase activation.

(a) Detailed view of the potential steric clash generated by the conformational change of EcCaspase upon N7-cADPR binding. Key residues are shown as sticks. (b) Structural alignment of N7-cADPR-free EcCaspase and inhibitor/substrate-free human caspase (PDB ID: 1K88). Four functional loops are labelled, and catalytic residues are displayed in sphere representations. (c) Structural superposition of N7-cADPR-free EcCaspase and inhibitor/substrate-bound human caspase (PDB ID: 1I51).



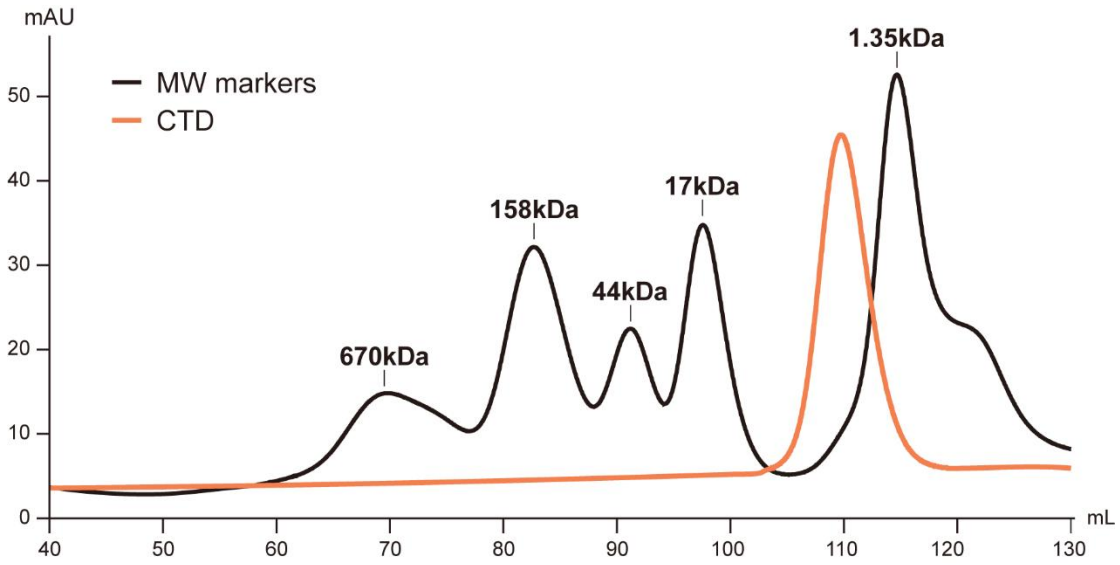
Supplementary Fig. S12 Activation of the type IV Thoeris system by viral capsid proteins.

(a) Schematic of the workflow to identify EcTIR-activating viral factors. (b) Mass spectrometry analysis identifying the EcTIR-interacting viral proteins.



Supplementary Fig. S13 Selection and characterization of T6 phage escape mutants.

(a) Schematic of the experimental workflow for selecting phage escape mutants against type IV Thoeris immunity. (b) Plaque assay showing resistance phenotypes of T6 escape mutants against bacteria expressing the type IV Thoeris system. Results are representative of three biological replicates. (c) Sequence alignment illustrating the nonsense mutation (resulting in a premature stop codon) identified in the escape mutants. (d-e) AlphaFold-predicted structures of the Mhp monomer and the Mhp hexamer. The location of residue L195 is indicated.



Supplementary Fig. S14 Size-exclusion chromatography curve of isolated CTD-containing EcCaspase.

The size-exclusion chromatography profile of CTD-containing EcCaspase is overlaid with molecular weight standards.

Supplementary Table S1. Cryo-EM data collection and refinement statistics

	MBP-fused EcCaspase filament (EMD-66441) (PDB 9X0S)	EcCaspase filament (EMD-81533) (PDB 27XF)	N7-cADPR-bound-EcCaspase dimer (EMD-66434) (PDB 9X0G)	N7-cADPR-bound-EcCaspase tetramer (EMD-66442) (PDB 9X0T)	N7-cADPR-bound-EcCaspase hexamer (EMD-66443) (PDB 9X0U)
Data collection and processing					
Magnification	165,000	165,000	165,000	165,000	165,000
Voltage (kV)	300	300	300	300	300
Electron exposure ($e^-/Å^2$)	50	50	50	50	50
Defocus range (μm)	-1.2 to -1.6	-1.2 to -1.6	-1.2 to -1.6	-1.2 to -1.6	-1.2 to -1.6
Pixel size (Å)	0.725	0.731	0.692	0.692	0.692
Symmetry imposed	*C1*	*C1*	*C1*	*C1*	*C1*
Initial particle images (no.)	710,768	1,019,901	904,181	904,181	904,181
Final particle images (no.)	153,241	263,342	148,812	54,124	42,976
Map resolution (Å)	2.84	2.60	2.79	2.86	2.89
FSC threshold	0.143	0.143	0.143	0.143	0.143
Map resolution range (Å)	2.0 to 4.0	2.0 to 4.0	2.0 to 4.0	2.0 to 4.0	2.0 to 4.0
Refinement					
Initial model used	AlphaFold	AlphaFold	AlphaFold	AlphaFold	AlphaFold
Model resolution (Å)	3.3	2.9	3.3	3.4	3.5
FSC threshold	0.5	0.5	0.5	0.5	0.5
Model resolution range (Å)	2.8 to 3.1	2.5 to 2.7	2.7 to 3.4	2.8 to 3.4	2.8 to 3.6
Map sharpening *B* factor ($Å^2$)	-91.6	-67.0	-99.0	-83.1	-79.2
Model composition					
Non-hydrogen atoms	37521	39952	4901	9802	14703
Protein residues	4815	5136	626	1252	1878
Nucleotides	0	0	0	0	0
B factors ($Å^2$)					
Protein	177.09	269.22	130.06	135.83	158.26
Nucleotides	-	-	-	-	-
R.m.s. deviations					
Bond lengths (Å)	0.005	0.006	0.005	0.005	0.005
Bond angles (°)	1.105	0.955	0.859	1.142	1.122
Validation					
MolProbity score	1.52	0.95	1.90	1.87	1.96
Clashscore	7.32	1.14	8.09	8.60	8.74
Poor rotamers (%)	0.90	0.75	1.73	1.73	2.06
Ramachandran plot					
Favored (%)	97.41	97.34	95.95	96.52	96.28
Allowed (%)	2.59	2.59	4.05	3.32	3.67
Disallowed (%)	0.00	0.08	0.00	0.16	0.05

Reference

1 Danecek, P. *et al.* Twelve years of SAMtools and BCFtools. *Gigascience* **10**, doi:10.1093/gigascience/giab008 (2021).

2 Cingolani, P. *et al.* A program for annotating and predicting the effects of single nucleotide polymorphisms, SnpEff: SNPs in the genome of Drosophila melanogaster strain w1118; iso-2; iso-3. *Fly (Austin)* **6**, 80-92, doi:10.4161/fly.19695 (2012).

3 Thompson, R. F., Iadanza, M. G., Hesketh, E. L., Rawson, S. & Ranson, N. A. Collection, pre-processing and on-the-fly analysis of data for high-resolution, single-particle cryo-electron microscopy. *Nat Protoc* **14**, 100-118, doi:10.1038/s41596-018-0084-8 (2019).

4 Punjani, A., Rubinstein, J. L., Fleet, D. J. & Brubaker, M. A. cryoSPARC: algorithms for rapid unsupervised cryo-EM structure determination. *Nat Methods* **14**, 290-296, doi:10.1038/nmeth.4169 (2017).

5 Zheng, S. Q. *et al.* MotionCor2: anisotropic correction of beam-induced motion for improved cryo-electron microscopy. *Nat Methods* **14**, 331-332, doi:10.1038/nmeth.4193 (2017).

6 Bepler, T. *et al.* Positive-unlabeled convolutional neural networks for particle picking in cryo-electron micrographs. *Nat Methods* **16**, 1153-1160, doi:10.1038/s41592-019-0575-8 (2019).

7 Abramson, J. *et al.* Accurate structure prediction of biomolecular interactions with AlphaFold 3. *Nature* **630**, 493-500, doi:10.1038/s41586-024-07487-w (2024).

8 Meng, E. C. *et al.* UCSF ChimeraX: Tools for structure building and analysis. *Protein Sci* **32**, e4792, doi:10.1002/pro.4792 (2023).

9 Emsley, P., Lohkamp, B., Scott, W. G. & Cowtan, K. Features and development of Coot. *Acta Crystallogr D Biol Crystallogr* **66**, 486-501, doi:10.1107/S0907444910007493 (2010).

10 Moriarty, N. W., Grosse-Kunstleve, R. W. & Adams, P. D. electronic Ligand Builder and Optimization Workbench (eLBOW): a tool for ligand coordinate and restraint generation. *Acta Crystallogr D Biol Crystallogr* **65**, 1074-1080, doi:10.1107/S0907444909029436 (2009).

11 Afonine, P. V. *et al.* Real-space refinement in PHENIX for cryo-EM and crystallography. *Acta Crystallogr D Struct Biol* **74**, 531-544, doi:10.1107/S2059798318006551 (2018).

12 Williams, C. J. *et al.* MolProbity: More and better reference data for improved all-atom structure validation. *Protein Sci* **27**, 293-315, doi:10.1002/pro.3330 (2018).

13 Nadendla, E. K., Tweedell, R. E., Kasof, G. & Kanneganti, T. D. Caspases: structural and molecular mechanisms and functions in cell death, innate immunity, and disease. *Cell Discov* **11**, 42, doi:10.1038/s41421-025-00791-3 (2025).